

# Origin of Anomalous Xe-H in Nanodiamond Stardust

K.-L. Kratz<sup>\*,†</sup>, K. Farouqi<sup>\*,\*\*</sup>, O. Hallmann<sup>\*</sup>, B. Pfeiffer<sup>‡</sup> and U. Ott<sup>\*,§</sup>

<sup>\*</sup>Max-Planck-Institut für Chemie, Otto-Hahn-Institut, D-55128 Mainz, Germany

<sup>†</sup>Fachbereich Chemie, Pharmazie und Geowissenschaften, Universität Mainz, Mainz, Germany

<sup>‡</sup>Department of Physics, Univ. of Notre Dame, Notre Dame, IN 4656556, USA

<sup>\*\*</sup>Zentrum für Astronomie der Universität Heidelberg, D-69120 Heidelberg, Germany

<sup>‡</sup>II. Physikalisches Institut, Univ. Gießen, D-35392 Gießen, Germany

<sup>§</sup>Univ. of West Hungary, H-9700 Szombathely, Hungary

**Abstract.** Still today, the nucleosynthesis origin of Xe-H in presolar nanodiamonds is far from understood. Historically, possible explanations were proposed by a secondary “neutron-burst” process occurring in the He- or C/O-shells of a type-II supernova (SN-II), which are, however, not fully convincing in terms of modern nucleosynthesis conditions. Therefore, we have investigated Xe isotopic abundance features that may be diagnostic for different versions of a classical, primary r-process in high-entropy-wind (HEW) ejecta of core-collapse SN-II. We report here on parameter tests for non-standard r-process variants, by varying electron abundances ( $Y_e$ ), ranges of entropies ( $S$ ) and expansion velocities ( $V_{exp}$ ) with their correlated neutron-freezeout times ( $\tau(\text{freeze})$ ) and temperatures ( $T_9(\text{freeze})$ ). From this study, we conclude that a best fit to the measured Xe-H abundance ratios  ${}^i\text{Xe}/{}^{136}\text{Xe}$  can be obtained with the high- $S$  “main” component of a “cold” r-process variant.

**Keywords:** ISM:abundances – nuclear reactions, nucleosynthesis, abundances – supernovae: general

**PACS:** 26.30.-k,26.50.+x,97.10.Cv,97.10.Tk

## 1. INTRODUCTION

Apart from the historical “bulk” Solar System (S.S.) isotopic abundances ( $N_{\odot}$ ) [1, 2, 3, 4] and the elemental abundances measured for metal-poor halo stars (for a review, see e.g. [5, 6]), meteoritic grains of stardust, which survived from times before the S.S. formed (see, e.g. [7, 8, 9]) represent the third group of “observables” crucial for our understanding of the various nucleosynthesis processes in stars. Within the realm of meteoritic grains, attempts to explain the origin of nanodiamonds have not progressed as much as the understanding of other types of stardust, such as for example SiC and oxide grains. A major problem is the small size (average  $\simeq 2.6$  nm), which does not permit classical single-grain isotopic measurements. Therefore, “bulk” samples (i.e. millions of tiny nanodiamond grains) have to be analyzed. In nanodiamonds, peculiar isotopic features have been observed in several trace elements, which seem to suggest a connection to SNe. These include Xe-HL [10, 11] (with enhancements of light (L) p- and heavy (H) r-isotopes relative to  $N_{\odot}$ ), Kr-H and Pt-H [11, 12] (where the heavy (H) isotopes are enhanced), and Te-H [13] (with a clear overabundance of the “r-only” isotopes). So far, nucleosynthesis processes suggested to account for the H r-process enhancements include “neutron-burst” scenarios of secondary nature [14, 15, 16], as well as a regular primary r-process augmented by an “early” separation between final, stable isotopes and radioactive isobars formed during the  $\beta$ -decay back to stability from the initial precursors in the assumed r-process path [17]. Since both earlier scenarios are not fully convincing, as a possible alternative we have initiated a concerted effort to look for isotopic features that may be diagnostic for non-standard variants of an r-process in high-entropy-wind (HEW) ejecta of core-collapse (cc) SNe (for details of the HEW scenario, see e.g. [18, 19, 20, 21]).

## 2. THE HEW R-PROCESS MODEL

The basic nucleosynthesis mechanisms for elements beyond Fe by slow (s-process) and rapid (r-process) captures of neutrons have been known for a long time [1, 2, 3]. However, the search for a robust r-process production site has proven difficult. Still today, all proposed scenarios not only face problems with astrophysical conditions, but also with the necessary nuclear-physics input for very neutron-rich isotopes. Among the various suggested sites, the neutrino-driven or high-entropy wind (HEW) of cc-SNe is one of the best studied mechanisms for a full primary

**TABLE 1.** Relevant r-process parameters for the formation of the  $A \simeq 130$  abundance peak with  $Y_e = 0.45$ , the respective full S-ranges and  $Y_n/Y_{seed} = 35$  for different r-process variants. All HEW calculations were performed with the theoretical nuclear-physics input based on the mass model ETFSI-Q [25, 26] and the local QRPA [27] improvements mentioned in the text.

$V_{exp}$ [km/s]	S [ $k_B$ /baryon]	maximum $2^{nd}$ r-peak	$\tau_r$ [ms] at neutron-freezeout	$T_9$	r-process variant
1000	370	A=130	560	1.23	hot & fast
2000	298		335	1.10	
4000	235		200	0.98	
6000	210	A=128	160	0.86	hybrid
8000	190		130	0.82	(standard)
10,000	175		110	0.79	
15,000	155		93	0.66	
20,000	140	A=126	78	0.60	cold & rapid

r-process already in the early Universe (see, e.g. [18, 19, 20, 21]). Nevertheless, also for this attractive scenario even in the most sophisticated hydrodynamical models the neutrino-driven HEW has been found to be proton-rich (electron fraction  $Y_e \geq 0.5$ ) during its entire life, thus precluding a rapid neutron-capture process (see, e.g. [22, 23]). However, recent work on charged-current neutrino interaction rates (see, e.g. [24]), seems to revive the HEW scenario by predicting that  $Y_e$  changes from an initially proton-rich value to moderately neutron-rich conditions with minimal values of  $Y_e \simeq 0.42$ .

Therefore, in the light of these recent findings, to us it appears to be justified of further using our parameterized, dynamical HEW approach, based on the initial model of Freiburghaus et al. [20], which assumes adiabatically expanding homogenous mass zones with different entropy (S) yields. This code has been steadily improved until today, for example to implement a better mathematical treatment for the tracking of the  $\beta$ -decaying nuclei back to stability with time-intervals small enough to consider late recaptures of previously emitted  $\beta$ -delayed neutrons, up to the longer-lived precursors 55-s  $^{87}\text{Br}$  and 24-s  $^{137}\text{I}$ .

As has been outlined in [21], in our HEW model the overall wind ejecta represent model-inherently weighted superpositions of S (and probably also  $Y_e$ ) components, where the main astrophysical parameters are correlated via the “r-process strength formula” ( $Y_n/Y_{seed} \simeq k_{SN} \times V_{exp} \times (S/Y_e)^3$ ). Following our traditional approach to find a possible explanation of the  $N_{r,\odot}$  “residuals” [4, 28], we have started the present study using our standard parameter combination of  $Y_e = 0.45$ ,  $V_{exp} = 7500$  km/s and the full S-range of  $20 \leq S \leq 280$   $k_B$ /baryon. As indicated in Table 1, under these conditions we have a “hybrid” r-process type with a neutron-freezeout temperature of  $T_9$ (freeze)  $\simeq 0.82$ , which is reached at a time  $\tau$ (freeze)  $\simeq 138$  ms after the r-process seed formation. This r-process variant reaches the maximum abundance at the  $A \simeq 130$  peak at  $S \simeq 195$  for  $Y_n/Y_{seed} \simeq 35$  with the top of the peak at  $A = 128$ . Thereafter, we have systematically investigated the whole astrophysics parameter space as functions of electron fraction ( $0.40 \leq Y_e \leq 0.495$ ), expansion velocity ( $1000 \leq V_{exp} \leq 30,000$  km/s) and entropy ranges. In Table 1, we show some relevant parameters for the formation of the  $A \simeq 130$  peak with  $Y_e = 0.45$  and the corresponding full S-ranges for different possible r-process variants, ranging from a “hot, fast” version with an r-process boulevard at moderate distance from the stability line, up to a “cold, rapid” process with r-progenitors far from stability.

### 3. REPRODUCTION OF THE XE-H ABUNDANCES

In the nanodiamond stardust samples, the Xe-H abundance pattern is given as ratios relative to the assumed “r-only” isotope  $^{136}\text{Xe}$ , and have (somewhat model dependent) values of  $^{129,131,132,134}\text{Xe}/^{136}\text{Xe} = 0.207, 0.178, 0.167, 0.699$  [11, 12]. As is shown in Fig. 1, these values are clearly different from the  $N_{r,\odot}$  abundance ratios of 3.37, 2.55, 2.24, 1.18 [28]. The low measured values of the three lighter (r+s) Xe isotopes indicate a significant reduction of their abundances by factors of 16.3, 14.3 and 13.4, respectively, whereas the abundance ratio of the two heavy “r-only” isotopes (96.2 % r  $^{134}\text{Xe}$  and 99.95 %  $^{136}\text{Xe}$ ) is only moderately changed by a factor 1.7. In the historical “neutron-burst” model of [14, 15], this Xe abundance pattern has been obtained by a neutron-capture shift of an s-processed seed composition in an explosive shell-burning scenario. In the HEW scenario, however, such a strong abundance shift

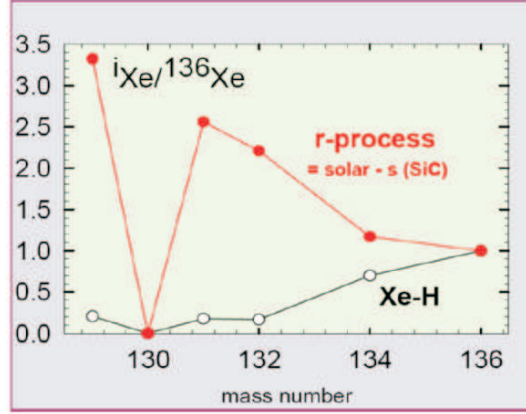


**FIGURE 1.** Isotopic composition of Xe-H compared to S.S. r-process Xe, adopted from [14]. The abundance ratios are normalized to “r-only”  $^{136}\text{Xe}$ .

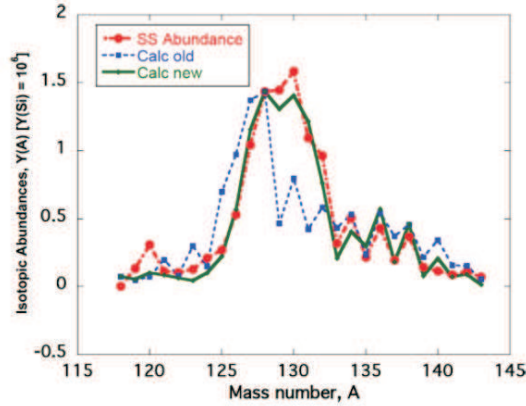


**FIGURE 2.** Observed S.S.-r abundance “residuals” ( $N_{r,\odot} = N_{\odot} - N_{s,\odot}$ ) [4, 28] (filled circles connected with a dot-dash line) along with the isotopic abundances calculated as described in the text, using older values for  $\beta$ -decay properties (filled squares connected with a dashed line) and recently updated  $\beta$ -decay half-lives and delayed neutron-branching ratios (filled diamonds connected with a solid line). The calculated values are normalized to the S.S.-r abundance of  $^{128}\text{Te}$ .

to a peak at  $N = 82$   $^{136}\text{Xe}$ , with its main r-progenitor  $N = 86$   $^{136}\text{Sn}$ , is very unlikely. It would require a drastic change of the position and height of the  $N_{r,\odot}$  peak with its classical, most abundant  $N = 82$  “waiting-point” isotopes  $^{128}\text{Pd}$ ,  $^{129}\text{Ag}$  and  $^{130}\text{Cd}$  (see, e.g. [27]),  $\beta$ -decaying to the stable isobars  $^{128}\text{Te}$ ,  $^{129}\text{Xe}$  and  $^{130}\text{Te}$ . Hence, if a primary rapid neutron-capture process would be the nucleosynthesis origin of the peculiar Xe-H pattern, possibilities within more likely non-standard r-process variants have to be investigated.

However, before studying the individual, and later also possible combined effects of the main HEW parameters  $Y_e$ ,  $V_{exp}$  and  $S$ , we first have to verify that our r-process model is able to reproduce the isotopic pattern of the whole  $N_{r,\odot}$  peak region. In this context, our experimental information on direct r-process progenitor isotopes as well as a detailed understanding of the nuclear-structure development in the  $N = 82$  magic-shell region (see, e.g. [27]) is essential. Only with both, realistic astrophysical and nuclear-physics parameters, a satisfactory agreement between S.S.-r observations and our HEW calculations can serve as a “basis” for the later interpretation of abundance patterns deviating from the standard  $N_{r,\odot}$  pattern. In Fig. 2, we show two fits of the  $120 \leq A \leq 140$  peak region, both with the nuclear-physics input based on the ETFSI-Q mass model, but the one with older theoretical  $\beta$ -decay properties, and the other with updated half-lives and  $P_{xn}$  values, as described in Arndt et al. [27]. With the latter, new nuclear-physics input, for the above mass range the mean abundance ratio of  $N_{r,calc}/N_{r,\odot} \simeq 0.90$ . To our knowledge, this is the best agreement one has been able to achieve so far for the region of the 2<sup>nd</sup> r-peak.

We now want to check the possible influence of the neutron-richness of the r-process ejecta on the  $^{i}\text{Xe}/^{136}\text{Xe}$

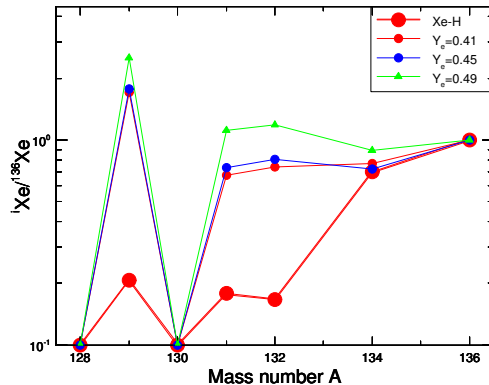


**FIGURE 3.** HEW predictions of  $^{129}\text{Xe}/^{136}\text{Xe}$  abundance ratios for r-process ejecta with different electron fractions  $Y_e$ , with a constant expansion velocity  $V_{exp} = 7500$  [km/s] and the respective full entropy ranges. The case  $Y_e = 0.49$  corresponds to only slightly neutron-rich conditions as observed for metal-deficient “r-poor” halo stars;  $Y_e = 0.45$  represents moderately neutron-rich ejecta as observed for “r-rich” stars; and  $Y_e = 0.41$  corresponds to strongly neutron-rich conditions. The Xe-H data are included for comparison. For further details, see text.

abundance ratios. Therefore, we vary the HEW parameter  $Y_e$ , i.e. the electron fraction, in the range  $0.41 \leq Y_e \leq 0.49$ , while keeping the wind expansion velocity  $V_{exp} = 7500$  [km/s] constant and taking the respective full entropy ranges (see also Table 1). In Fig. 3, we show three typical results in comparison with the Xe-H measurements [11]. Here, the case  $Y_e = 0.49$  corresponds to only slightly neutron-rich conditions, as observed for r-process poor “Honda-type” halo stars (e.g. HD 122563 [29]);  $Y_e = 0.45$  represents moderately neutron-rich conditions for r-process enriched, metal-deficient “Snedden-type” stars (e.g. CS 22892-052 [30]); and  $Y_e = 0.41$  corresponds to strongly neutron-rich, “Cayrel-type” stars (e.g. CS 31082-001 [31]), which show a “main” r-process component with a so-called “actinide boost”. As can be seen from Fig. 3, the measured low Xe abundance ratios are not met by varying the electron fraction parameter alone. But, the trend shows that high  $Y_e$  values may be less likely than the lower ones. Therefore, we conclude that the Xe-H pattern seems to favor neutron-rich HEW ejecta.

In a second step, we vary the individual parameter of the HEW expansion velocity  $V_{exp}$  in the range  $1000 \leq V_{exp} \leq 30,000$  [km/s], while now keeping the electron fraction  $Y_e = 0.45$  constant and taking again the full respective entropy ranges (see also Table 1). In Fig. 4, we show again three typical results in comparison with the Xe-H data [11]. Here, the case  $V_{exp} = 7500$  [km/s] corresponds to our “standard” HEW parameter combination for a “hybrid” r-process [21];  $V_{exp} = 3000$  [km/s] represents a moderately fast, “hot” r-process; and  $V_{exp} = 15,000$  [km/s] corresponds to a rapid, “cold” r-process variant (for further details, see [21]). As is evident from this figure, again the measured Xe-H abundance ratios are not met by varying the ejection velocities of the r-process ejecta alone. However, the trend in this case indicates that relatively high  $V_{exp}$  values may be more likely than low ones. What we do not show here, is our further result that very high  $V_{exp} \geq 20,000$  [km/s] may, however, be excluded too. Therefore, we conclude from this HEW parameter choice that the Xe-H pattern seems to favor rapid, neutron-rich, “cold” r-process ejecta.

The last HEW parameter to “play” with in our present study is the range of the superimposed entropy ( $S$ ) components. From [21] we know that with increasing  $S$ , we can distinguish between three different primary, rapid nucleosynthesis components. In the lowest  $S$ -range, where the HEW has no or not yet enough “free neutrons” ( $Y_n/Y_{r-seed} \leq 1$ ) we have a charged-particle process. For somewhat higher  $S$ -values, a relatively low fraction of “free neutrons” ( $1 \leq Y_n/Y_{r-seed} \leq 20 - 30$ ) occurs, which leads to a “weak” neutron-capture process that produces r-matter up to the rising wing of the  $A \simeq 130$  peak. And finally, for high  $S$ -values (and moderately low  $Y_e$ ; see above) high neutron fractions of up to  $Y_n/Y_{r-seed} \simeq 150$  can be obtained, under which conditions a “main” r-process component becomes possible. This r-component forms a robust S.S.-r like REE “pygmy peak”, the full  $A \simeq 195$  peak, and may reach up to the Th and U r-chronometer isotopes.

Given this development of  $S$  and  $Y_n/Y_{r-seed}$ , it is immediately evident that the r-process Xe isotopes between  $^{129}\text{Xe}$  and  $^{136}\text{Xe}$  are predominantly produced by the “main” component, which (quite logically) suggests to cut out the low- $S$  ranges of the charged-particle and the “weak-r” components. Furthermore, a closer look to the production of the individual Xe isotopes as a function of  $S$  shows, that they are formed under slightly different conditions. The most significant differences occur for the lightest r-isotope  $^{129}\text{Xe}$ , which is placed in the left part of the top of the 2<sup>nd</sup> r-

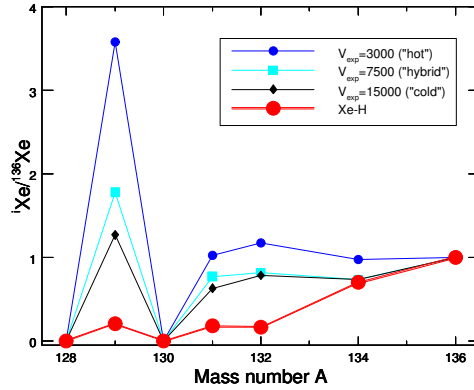


**FIGURE 4.** HEW predictions for  $^{135}\text{Xe}/^{136}\text{Xe}$  abundance ratios for neutron-rich r-process ejecta with different expansion velocities  $V_{exp}$ , with a constant electron fraction  $Y_e = 0.45$  and the respective full entropy ranges. The case  $V_{exp} = 7500$  [km/s] represents our “standard” parameter combination for a “hybrid” r-process;  $V_{exp} = 3000$  [km/s] corresponds to a fast, “hot” r-process; and  $V_{exp} = 15,000$  [km/s] represents a rapid, “cold” r-process variant. For comparison, again the Xe-H data are included. For further details see text and [21].

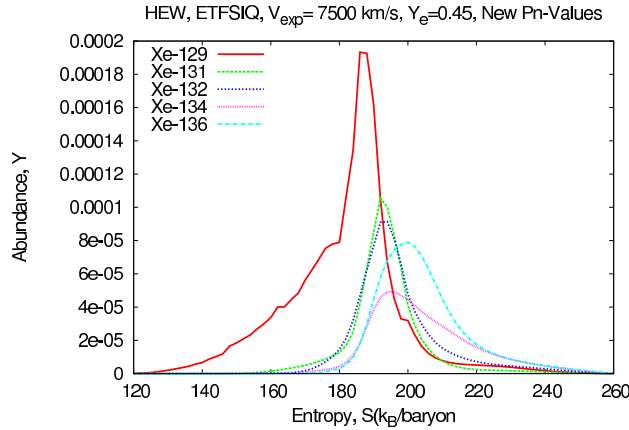


**FIGURE 5.** Xe abundances ( $Y$ ) of HEW ejecta for our “standard” parameter combination of  $Y_e = 0.45$  and  $V_{exp} = 7500$  [km/s] as a function of entropy  $S$  [ $k_B/\text{baryon}$ ]. The Xe isotopes are produced in slightly different  $S$ -ranges, where  $^{129}\text{Xe}$  abundance maximum occurs at a lower entropy that those for the heavier isotopes. For further details, see text.

peak, and the heaviest r-nuclide  $^{136}\text{Xe}$ , which sits already beyond the right, decreasing wing of the peak, close to the beginning of the REE region. For our “standard” HEW parameter combination of  $Y_e = 0.45$  and  $V_{exp} = 7500$  [km/s], this situation is shown in Fig. 5. From this figure, it can be seen that  $^{129}\text{Xe}$  is mainly produced at entropies of  $S \leq 190$  (by the initial, classical  $N = 82$  r-process “waiting-point” nuclide  $^{129}\text{Ag}$ ), whereas the heavier Xe isotopes need higher entropies.

This picture now suggests to check the effect of selecting only the high- $S$  components out of the full  $S$ -range. Again, for our “standard” HEW parameter combination for  $Y_e$  and  $V_{exp}$ , this is shown in Fig. 6. We see that in particular the high “overabundance” of  $^{129}\text{Xe}$  can be nicely reduced by the requested order of magnitude, while the abundance ratio of the two “r-only” isotopes  $^{134}\text{Xe}$  and  $^{136}\text{Xe}$  remains practically unaffected. From this result, our near-final conclusion is that the measured Xe-H pattern seems to be the signature of a moderately neutron-rich, “hybrid, main” (or even “strong”) r-process variant.

After we have so far studied the effects of the main individual HEW parameters, and have determined their possible optimum values, at the very end we can combine these values and compare the respective abundance predictions to the measured Xe-H pattern. This is shown in our final Fig. 7 for a limited number of “best fit” combinations of  $Y_e \simeq 0.43$ , the respective low- $S$  cuts and a range of reasonable, but not too high  $V_{exp}$  values. Similar to our result already obtained

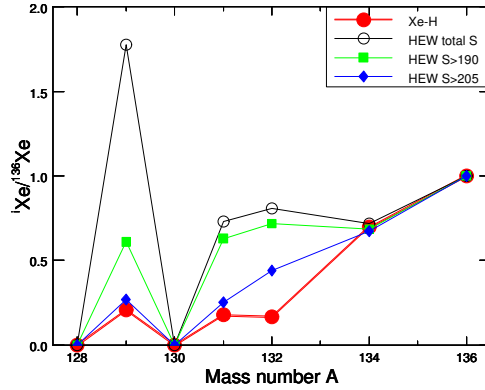


**FIGURE 6.** HEW predictions of  $i\text{Xe}/^{136}\text{Xe}$  abundance ratios for different entropy ranges, with constant “standard” r-process conditions of  $Y_e = 0.45$  and  $V_{exp} = 7500$  [km/s], compared to the measured Xe-H data. The results obtained with the cuts of the low-S ranges, in particular the “best fit” for  $S \geq 205$ , represent the signature of a moderately neutron-rich “hybrid, main” r-process variant. For comparison, again the Xe-H data are included. For further discussion, see text.

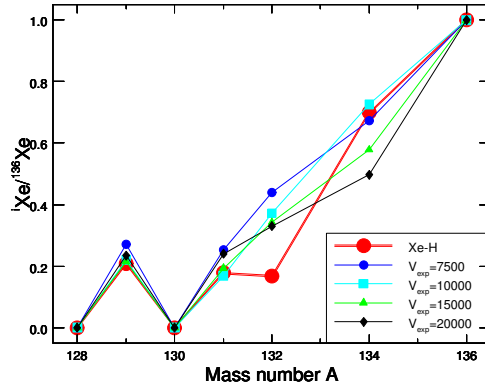


**FIGURE 7.** HEW predictions of  $i\text{Xe}/^{136}\text{Xe}$  abundance ratios, combining the “best” individual astrophysics parameters for  $Y_e \simeq 0.43$  and the respective S-cuts with different choices of  $V_{exp}$ . “Best fit” conditions are obtained for somewhat higher expansion velocities than our standard value, in the range  $10,000 \leq V_{exp} \leq 15,000$  [km/s]. For further discussion, see text.

from the parameters used in Fig. 6, we conclude that the Xe-H abundance ratios indicate its presolar formation by a “rapid, cold, main” r-process variant. The measured abundance ratios of  $^{129,131,134}\text{Xe}/^{136}\text{Xe}$  are well reproduced within 20 to 30 %. Only the value of  $^{132}\text{Xe}/^{136}\text{Xe}$  remains too high by about a factor 2.5. It is interesting to note in this context, that also the historical “neutron-burst” model [14, 15] predicted a somewhat too high abundance of  $^{132}\text{Xe}$ .

Finally, it is worth to be mentioned that preliminary results for platinum indicate that the HEW conditions found to be favorable for Xe-H can also account for the reported Pt-H in presolar diamonds [11, 12]. With Xe-H lying in the  $A \simeq 130 N_{r,\odot}$  peak and Pt-H in the  $A \simeq 195$  peak, these cosmochemical samples with their isotopic abundance patterns can provide constraints on the astrophysical conditions for the production of a full, “main” r-process, which cannot be deduced with this sensitivity by the elemental abundance patterns of metal-poor halo stars.

## REFERENCES

1. E.M. Burbidge et al. (B<sup>2</sup>FH), *Rev. Mod. Phys.* **29**, 547 (1956).
2. A.G.W. Cameron, *PASP* **69**, 201 (1957).

3. C.D. Coryell, *Ann. Prog. Rep. MIT*, **VI Nucl. Chemistry**, 29 (1956); and *Journal of Chemical Education* **38**, 67 (1961).
4. K. Lodders, H. Palme and H.-P. Gail, *Landolt-Börnstein, New Series VI/4B-34*, 1 (2009).
5. C. Sneden, J.J. Cowan and R. Gallino, *ARA&A* **46**, 241 (2008).
6. M. Spite and F. Spite, *Astron. Nachr.* **No. 1**, 1 (2014).
7. D.D. Clayton and L.R. Nittler, *ARA&A* **42**, 39 (2004).
8. K. Lodders and S. Amari, *ChEG* **65**, 93 (2005).
9. E. Zinner, Update in: *Treatise on Geochemistry*, Oxford: Elsevier Ltd., 1.02, 1 (2004).
10. G.R. Huss and R.S. Lewis, *Meteoritics* **29**, 791 (1994).
11. U. Ott et al.,; *MAPS* **44**, A162 (2009); and *PASA* **29**, 90 (2012).
12. U. Ott et al., *Meteoritics* **45**, A159 (2010)
13. S. Richter, U. Ott and F. Begemann, *Nature* **391**, 261 (1998).
14. D.D. Clayton, *Ap.J.* **340**, 613 (1989).
15. B.S. Meyer, D.D. Clayton and L.S. The, *Ap.J.* **540**, L49 (2000).
16. T. Rauscher et al., *Ap.J.* **576**, 323 (2002).
17. U. Ott, *Ap.J.* **463**, 344 (1996).
18. S.E. Woosley et al., *Ap.J.* **433**, 229 (1994).
19. K. Takahashi, J. Wittl and H.-T. Janka, *A&A* **286**, 857 (1994).
20. C. Freiburghaus et al., *Ap.J.* **516**, 381 (1999).
21. K. Farouqi et al., *Ap.J.* **694**, L49 (2009); and *Ap.J.* **712**, 1359 (2010).
22. T. Fischer et al., *A&A* **517**, 80 (2010).
23. L. Hüdepohl et al., *Phys. Rev. Lett.* **104**, 251101 (2010).
24. L.F. Roberts, S. Reddy and G. Shen, *Phys. Rev.* **C86**, 065803 (2012).
25. J.M. Pearson, R.C. Nayak and S. Goriely, *Phys. Lett.* **B387**, 455 (1996)
26. P. Möller, B. Pfeiffer and K.-L. Kratz, *Phys. Rev.* **C67**, 055802 (2003).
27. O. Arndt et al., *Phys. Rev.* **C84**, 061307 (2011).
28. S. Bisterzo et al., *MNRAS* **418**, 284 (2011).
29. S. Honda et al., *Ap.J.* **666**, 1189 (2007).
30. C. Sneden et al., *Ap.J.* **591**, 936 (2003).
31. V. Hill et al., *A&A* **387**, 560 (2002).